RSC Advances

ROYAL SOCIETY OF CHEMISTRY

www.rsc.org/advances

RSC Advances

ARTICL

Preparation and Its Application of Hollow $ZnFe_2O_4$@PANI Hybrids as High Performance Anode Materials for Lithium-Ion Batteries

Ke Wang[(a)], Ying Huang*[(a)], Duo Wang[(a)], Yang Zhao[(b)], Mingyue Wang[(a)],Xuefang Chen[(a)] ,Xiulan Qin[(a)], Suping Li[(a)]

Abstract: $ZnFe_2O_4$, a kind of mixed transition metal oxides, are considered as one of the most attractive potential anode materials for LIBs due to their high reversible capacity and satisfactory structural stability. However, the low conductivity and the serious volume exchange during the electrochemical process are still two main issues for $ZnFe_2O_4$. In this study, we firstly designed the conductive PANI layer coated hollow $ZnFe_2O_4$ nanospheres by a micro emulsion polymerization. Two strategies of hollow structure and PANI coating are attempted to relieve expansion and increase conductivity. The results show that as-designed hollow $ZnFe_2O_4$ @PANI composites exhibit a large initial specific capacity of 1489.38mAh g^{-1} at first discharge that is maintained at over 607.3 mAh g^{-1} even after 50 charge-discharge cycles.

Key words: $ZnFe_2O_4$; PANI layer; hollow structure; anode materials; electrochemical process

Introduction

Rechargeable lithium-ion batteries (LIBs), as the dominant attractive secondary batteries, have achieved a great commercial success in portable electronic-equipments, electric vehicles, and stationary energy storage systems. However, the specific energy of present lithium ion batteries is still insufficient for many applications due to the limited specific charge capacity of the anode materials [1-6]. To some extent, the widely used conventional graphite as anode material is one of the key technical barriers [7, 8], because of its relatively low specific capacity (372 mAh g^{-1}) and poor safety. In the past decade, transition metal oxides such as Fe_3O_4 [9, 10], $NiFe_2O_4$ [11], $CoFe_2O_4$ [12], $ZnCo_2O_4$ [13], and $ZnFe_2O_4$ [14] have been stood out among the most widely investigated anode materials of LIBs. Of the transition metal oxides, zinc ferrite ($ZnFe_2O_4$) has received large research efforts due to its low cost and high safety [15], as well as the high theoretical specific capacity (1072 mAh g^{-1}) [16-18], its poor electrical conductivity and large volume expansion, however, limit its practical application.

To solve these problems, common strategies such as introducing conductive agents and fabricating nanometer-sized $ZnFe_2O_4$ have been used [19-21]. Many approaches including carbon-based material coating [22, 23], element doping [24] and special structure preparation [25] also have been devoted to improve the electrochemical performance of $ZnFe_2O_4$. Thereinto, conductive polymers and inorganic oxide nanocomposites have appealed great attention because of their unique structure [26], microwave absorption properties [27], and especially the wide range of potential uses as battery anodes [28]. In addition, hollow micro-nanostructured particles have gained growing interests owing to the hollow structure provides a superior configuration for accommodating the volume change and facilitates the electron and ion transfer [29].

Here, we firstly design and fabricate PANI layer coated hollow $ZnFe_2O_4$ nanospheres via hydrothermal and subsequent emulsion polymerization methods. The as-prepared nanocomposites present two structural superiorities, in which the hollow inner can reduce the internal stress during electrochemical process and the PANI layer can effectively enhance the conductivity. In this case, the hollow $ZnFe_2O_4$@PANI composites exhibits excellent cycling performances and rate properties compared with bare $ZnFe_2O_4$.

Results and discussion

Fig. 1(a) shows the XRD patterns of $ZnFe_2O_4$ nanospheres and hollow $ZnFe_2O_4$@PANI composites. The patterns (i) are identified as spinel $ZnFe_2O_4$ with the lattice parameters of a cubic structure (space group Fd3m, JCPDS card no. 82-1049). The diffraction peaks corresponding to 2θ values of 18.42°, 30.10°, 35.72°, 37.06°, 42.98°, 53.33°, 56.79°,62.41°, and 73.77° are confirmed as the planes (111), (220), (311), (222), (400), (422), (511), (440), and (533), respectively. The diffraction peaks of hollow $ZnFe_2O_4$@PANI composites (ii) are in agreement with the standard data of the hollow $ZnFe_2O_4$ nanospheres, and the diffraction peaks of PANI cannot be detected, which suggests that its little content and it's non-crystalline structure. To investigate the content of PANI in the as-synthesized composites, TGA analysis has been carried out in an air atmosphere, as shown in

a. Department of Applied Chemistry and The Key Laboratory of Space Applied Physics and Chemistry ,Ministry of Education, School of Science, Northwestern Polytechnical University, Xi'an 710072, PR China
E-mail: yingh@nwpu.edu.cn; ky131419@yahoo.com
b. Department of Mechanical and Materials Engineering, University of Western Ontario, London, Ontario, N6A 5B9, Canada

RSC Advances

ARTICL

Fig. 1(b). The weight loss before 100 °C is attributed to the release of the absorbed water. The rapid mass loss occurring between 200 and 700 °C is ascribed to the decomposition of PANI in air. Therefore, according to the change of weight, it is estimated that the amount of the $ZnFe_2O_4$ and PANI in the composites is 69.27wt% and 30.83%, respectively.

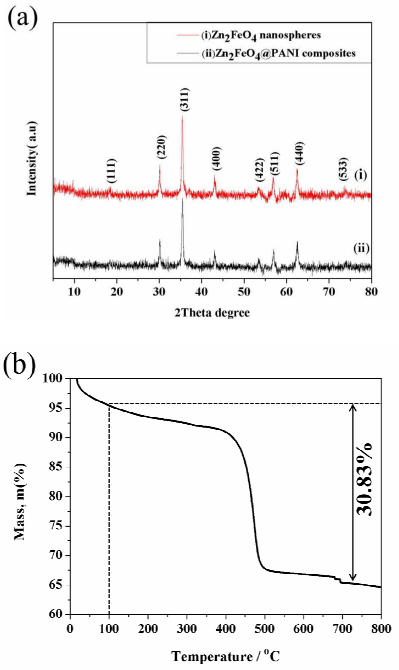

Fig.1 (a) XRD patterns of hollow $ZnFe_2O_4$ nanospheres and hollow $ZnFe_2O_4$@PANI composites; (b) the TGA curve of hollow $ZnFe_2O_4$@PANI composites

To further understand the surface chemical composition of the hollow $ZnFe_2O_4$@PANI composites. The XPS spectrum of the composite was conducted and the results are shown in Fig. 2. In Fig. 2(a), the Zn 2p spectrum can be de-convoluted into two distinct curves, related to the binding energies of Zn $2p_{3/2}$ and Zn $2p_{1/2}$, indicating the oxidation state of Zn^{2+} in the sample [29]. Meanwhile, the Fe 2p spectrum in Fig. 2(b) indicate the peaks at binding energies of 711.93 eV (Fe $2p_{3/2}$) and 724.83 eV (Fe $2p_{1/2}$) with a shake-up satellite at 718.48 eV. The observed Zn 2p and Fe 2p photoelectron peaks are consistent with the peaks reported for Zn^{2+} and Fe^{3+} in the $ZnFe_2O_4$. In Fig. 2(c), the de-convoluted XPS peak of O 1s centered at the binding energy of 530.43 eV is consistent with the O^{2-} anion from the $ZnFe_2O_4$, while the peaks with the binding energies of 531.88 eV and 533.13 eV relate to oxygen bonded to contaminated carbon (C -O, C=O) [30]. In Fig. 2(d), the N 1s spectrum of PANI can be de-convoluted into three distinct curves, related to different nitrogen forms. The peak appearing at 398.9 eV is corresponded to imine (N=) [31], and the peak at 400.1 eV may be assigned to protonated amine (NH^{2+}) [32]. The high binding energy of N^+ at 401.2 eV is due to the interaction between N^+ and protons introduced by the acid dopant. The test results are consistent with the data as demonstrated in literature [33].

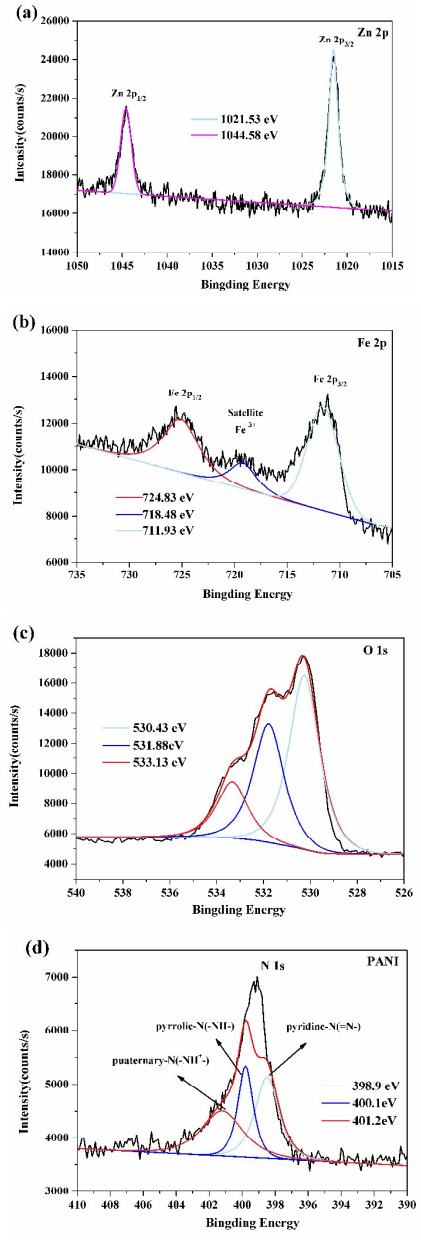

Fig.2 XPS spectra of (a) Zn 2p, (b) Fe 2p, (c) O 1s, and (d) PANI for hollow $ZnFe_2O_4$@PANI composites

Fig.3 (a, b) shows the SEM images of the as-prepared hollow

RSC Advances

ARTICL

$ZnFe_2O_4$ nanospheres. The pure $ZnFe_2O_4$ particles are consist of tiny particles with porous structure and each nanosphere exhibits a spherical shape with a fairly narrow size distribution. TEM analysis (Fig.3 (c)) is used to observe the interior space of the hollow nanospheres directly which demonstrates that the average sizes of nanospheres ranges from 200 to 300 nm. Fig. 3(d) gives the lattice resolved HRTEM image of $ZnFe_2O_4$. The fringe spacings of 0.26 nm correspond to the interplanar distance of (311) planes of $ZnFe_2O_4$. The HRTEM image further confirms that the primary particles sizes are around 20 nm and porous gaps between each particle, which is consistent with SEM results.

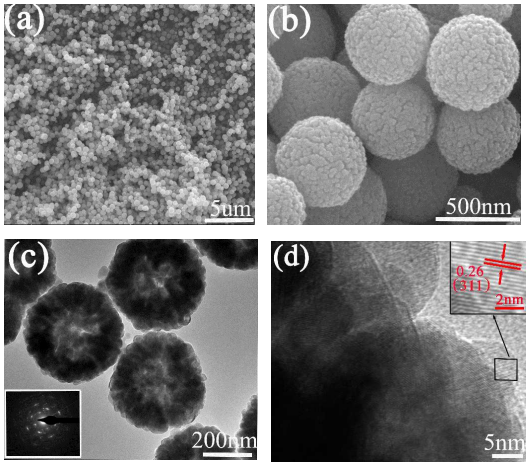

Fig.3 (a), (b) SEM images of hollow $ZnFe_2O_4$ nanospheres, (c) TEM and (d) HRTEM images of hollow $ZnFe_2O_4$ nanospheres

The morphology of hollow $ZnFe_2O_4$@PANI composites was conducted by SEM and TEM images. The SEM image shown in Fig. 4(a) suggests that the particles are also formed with sphere-like shape with a rougher surface. These nanospheres appear to be well-distributed with an average diameter of about 350 nm. From TEM images in Fig. 4(b, c), it is found that a distinguished core–shell structure is formed. The light-colored layers of PANI with amorphous structure are successful coated on the $ZnFe_2O_4$ nanospheres, and the thin coating layer displays a thickness about 30 nm. The high conductive PANI coating layer can be the key factor for the enhancement of electrochemical performances not only because the conductivity of the composites can be improved but also can play as the buffering materials due to the flexibility of it.

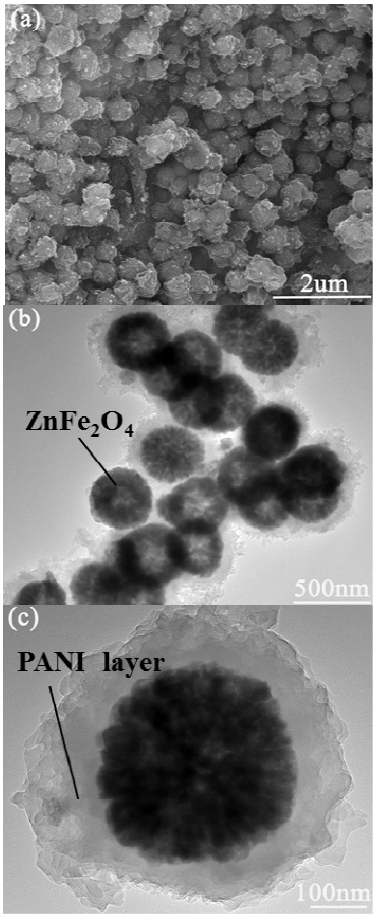

Fig. 4 SEM and TEM images of hollow $ZnFe_2O_4$@PANI composites

The N_2 adsorption–desorption measurement at a liquid N_2 temperature of -196 °C was used to further study the textural properties of the unique nanocrystalline hollow $ZnFe_2O_4$@PANI composites(Fig.5). According to the IUPAC classification, both of the samples presented a type IV isotherm with a type H3 hysteresis loop, indicating a typical mesoporous structure [34]. As seen, the BET specific surface areas of two samples are about 132.71 $m^2 g^{-1}$ and 178.84 $m^2 g^{-1}$. The increase of the surface area from hollow $ZnFe_2O_4$ nanospheres to hollow $ZnFe_2O_4$@PANI composites is probably due to the 2D hierarchical structures of conductive PANI coating layer. The pore size distribution in Fig. 5(a) (inset) demonstrates that hollow $ZnFe_2O_4$ nanospheres had much smaller pore volume (0.196 $cm^3 g^{-1}$ as a comparison of 0.241 $cm^3 g^{-1}$ for hollow $ZnFe_2O_4$@PANI composites) and a bimodal pore size distribution of around 3.74 nm and 7.75 nm as a comparison of 3.43 nm for hollow $ZnFe_2O_4$@PANI composites. However, the BET curve of hollow $ZnFe_2O_4$@PANI composite is not closed at low pressures, due to there was

RSC Advances

ARTICL

irreversible adsorption reaction in the low pressure zone.

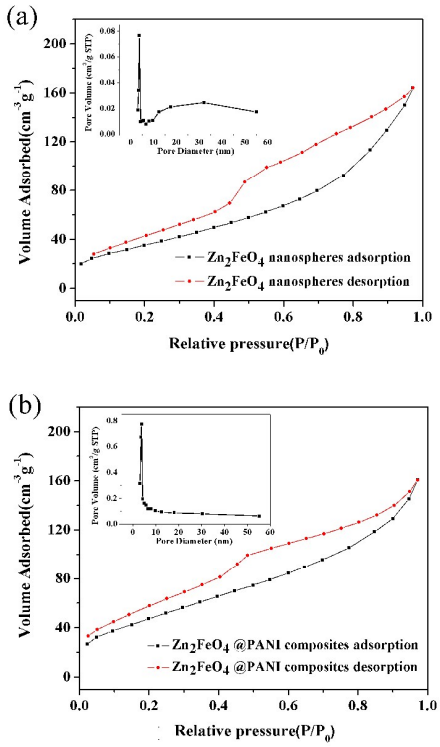

Fig.5 N_2 adsorption/desorption isotherms and pore-size distributions of hollow $ZnFe_2O_4$ nanospheres (a), and hollow $ZnFe_2O_4$@PANI composites (b).

As shown in Fig.6 (a), the lithium storage capacity of hollow $ZnFe_2O_4$@PANI composites are examined by galvanostatic discharge-charge cycling between 0.05 and 2.0 V at the current density of 300 mA g^{-1}. Results show that the first discharge-charge capacities of the hollow $ZnFe_2O_4$@PANI composites are 1489.38 and 949.25 mAh g^{-1}. A weak shoulder at about 0.9 V and an intensive peak at 0.64 V on the 1st cathodic curve are ascribed to the lithiation of $ZnFe_2O_4$ (eqn (1)), which gives metallic Zn and Fe irreversibly, as well as the formation of Li–Zn alloy (eqn (2)) [35]. Notably, the 2nd cathodic curve drops from open circuit voltage to 1.1 V takes place in the first lithiation process, which is associated with the phase transition from $ZnFe_2O_4$ to $LixZnFe_2O_4$ (x ~ 0.5) [36]. In contrast, only a voltage plateau is plateau is observed at 1.5-2.2 V in the delithiation processes.

$$ZnFe_2O_4 + 8Li^+ + 8e^- \rightarrow Zn + 2Fe + 4Li_2O \quad (1)$$

$$Zn + Li^+ + e^- \rightarrow LiZn \quad (2)$$

The unique hollow structure and the addition of PANI create the synergic effects. The hollow $ZnFe_2O_4$@PANI composites show the superior electrochemical performance than the hollow $ZnFe_2O_4$ nanospheres. Cycling properties of hollow $ZnFe_2O_4$ nanospheres and the hollow $ZnFe_2O_4$@PANI composites with a current density of 300 mA g^{-1} are displayed in Fig.6 (b). As seen, the pure $ZnFe_2O_4$ nanospheres of the discharge and charge capacities are 1126.6 and 728.6 mAh g^{-1} in the initial cycle, decreasing along with the following cycles, and then a low value of 292.5 mAh g^{-1} after 50 cycles. Such a large loss for the pure $ZnFe_2O_4$ electrode may result from the poor kinetics of electrochemical conversion reaction. The capacity of the hollow $ZnFe_2O_4$@PANI electrode decreased within the first 7 cycles before reached a relatively stable value thereafter; and eventually maintained the discharge capacity of 607.3 mAh g^{-1} after 50 discharge/charge processes. These results indicate the important role of PANI thin layer in the cycling characteristic of the $ZnFe_2O_4$-based anodes.

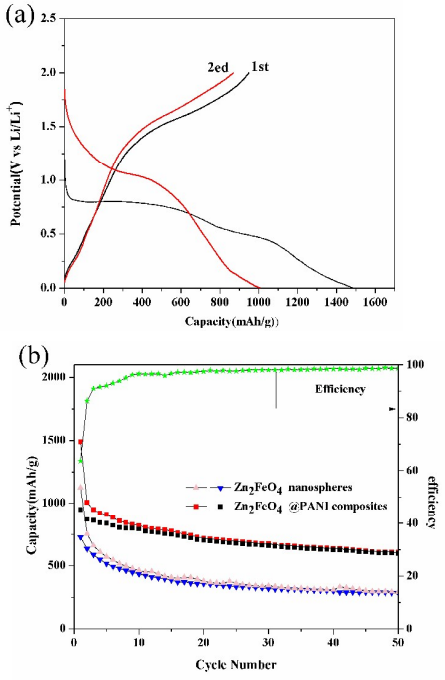

Fig.6 (a) Galvanostatic lithiation-delithiation profiles of the hollow $ZnFe_2O_4$@PANI composites electrode for different cycles at: 1st cycle and 2nd cycle, these tests are conducted at a current density of 300 mA g^{-1} between 0.01 and 2.0 V; (b) comparative cycling performance of hollow $ZnFe_2O_4$@PANI composites with hollow $ZnFe_2O_4$ nanospheres.

Fig. 7(a) reveals the CV plots of hollow $ZnFe_2O_4$@PANI composites scanned at 0.2 mV s^{-1} between 0.01 and 3.00 V (vs. Li/Li^+) for the first five cycles. A large reduction peak at around 0.75 V can be observed during the first cathodic scan, corresponding to the irreversible conversion from $ZnFe_2O_4$ to LiZn/Fe/Li_2O upon Li uptake. Meanwhile, the anodic peak is located near 2.59 V, corresponding to the oxidation of the transition metal to the metallic cation [37], and

RSC Advances

ARTICL

the anodic peak at 1.7 V was observed in the first cycle and could be attributed to the oxidation of the metallic iron and zinc into ZnO and Fe_2O_3. In the following cycles, there is no substantial change in the peak potentials, the negative electrode peaks are slightly moved to the right, while anodic peaks become more apparent in the following cycles. To clarify the different electrochemical behaviors of the two materials, we carried out electrochemical impedance spectroscopy (EIS) measurements. Fig. 7(b) shows EIS analysis of the electrodes of the hollow $ZnFe_2O_4$@PANI composites and hollow $ZnFe_2O_4$ nanospheres at 0.5 V from 0.01 Hz to 100 kHz after 50 cycles. In the equivalent circuit diagram, Rs is the electrolyte resistance and Rf represents the SEI resistance. W is associated with the Warburg impedance corresponding to the diffusion process of lithium-ions into the bulk of the electrode materials. CPE1 and CPE2 are two constant phase elements refer to the interfacial resistance and charge–transfer resistance, respectively. Rct is the charge–transfer resistance [36]. As seen Figure 7b, the EIS curve of hollow $ZnFe_2O_4$ is not continuous around X=75, which is caused by electrode materials' fluctuation in intermediate-frequency section. A comparison of the diameters of the semicircles indicates that the hollow $ZnFe_2O_4$@PANI composites is smaller than that of hollow $ZnFe_2O_4$ nanospheres, indicating the resistance dramatically decreases after the PANI content is increased in composite structure. Therefore, the facts confirm that the PANI coating can not only provide the high conductivity of the pure $ZnFe_2O_4$ electrode but also enhance the reactivity of the lithium ion toward electrode.

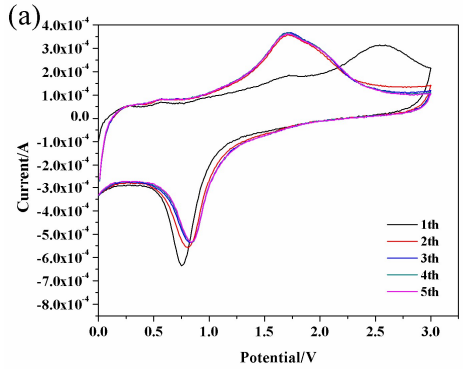

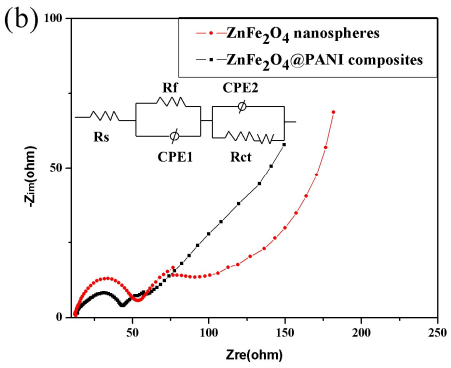

Fig.7 (a) Cyclic voltammetry of the hollow $ZnFe_2O_4$@PANI composites between 0.01 and 3.0 V at a scan rate of 0.2 mV s^{-1}; (b) EIS of the hollow $ZnFe_2O_4$@PANI composites and hollow $ZnFe_2O_4$ nanospheres before cycling (0.01–100 kHz), including the equivalent circuit model of the studied system.

The rate propertie of the hollow $ZnFe_2O_4$@PANI composites at different charge current densities are shown in Fig. 8. When increasing the current density to 600, 800 and 1200 mA g^{-1}, the hollow $ZnFe_2O_4$@PANI composites still can keep a discharge (charge) capacity of 822.65 (793.55), 578(560.9) and 502.8 (486.5) mAh g^{-1} up to 50 cycles, respectively. Even at high current densities of 1800 mA g^{-1}, the charge capacity can be kept at 410.2 mAh g^{-1} after 50cycles, higher than the theoretical capacity of graphite (372 mAh g^{-1}), displaying its excellent high-rate cycling stability. The improved electrochemical performance of the hollow $ZnFe_2O_4$@PANI composites can be attributed to the following two points. Firstly, the special nanostructures of the hollow $ZnFe_2O_4$@PANI composites can alleviate the pulverization problem and enhance the cycling performance. Additionally, the amorphous PANI in the composites are able to provide free space to buffer the release of the stress caused by the drastic volume variation during the conversion process.

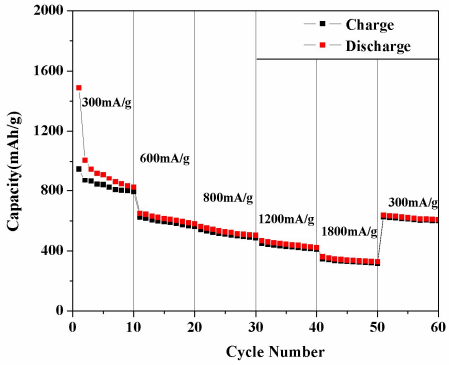

Fig.8 Rate capability of the hollow $ZnFe_2O_4$@PANI composites which is obtained between 0.01 and 2.0 V at various current densities.

Experimental Section

RSC Advances

ARTICL

Sample of hollow $ZnFe_2O_4$ nanospheres: the hollow $ZnFe_2O_4$ nanospheres were prepared through hydrothermal method. The process began with dissolving $FeCl_3$ (20 mmol), $Zn(Ac)_2{\cdot}2H_2O$ (10 mmol) and 8 g sodium acetate (NaAc) into 160 mL ethylene glycol to form well-distributed solutions. The hybrid complex was transferred into a 200 mL Teflon-lined stainless autoclave with a fill factor of approximately 70%. The autoclave was sealed and maintained in a furnace at 200 °C for 24 h. Then, the product was separated and washed for several times with deionized water and ethanol after the hydrothermal reaction was terminated. After these, the product was dried under vacuum at 60 °C for 12 h to obtain the hollow $ZnFe_2O_4$ nanospheres.

Sample of hollow $ZnFe_2O_4$@PANI composites: The hollow $ZnFe_2O_4$@PANI composites were synthesized by a micro emulsion polymerization way. Firstly, the monomer aniline (the molar ratio of aniline to hollow $ZnFe_2O_4$ nanospheres was 2:1) was added into the flask with the solution of $C_{18}H_{29}SO_3Na$ (0. 1 g) and the pH value was adjusted to 1-2. Then $ZnFe_2O_4$ and N-butanol (0.2 ml) were added into the solution with stirring for 1 h to form microemulsion. Afterward, $(NH_4)_2S_2O_8$ water solution (the molar ratio of APS/aniline was fixed at 1:1) was slowly dropped into the liquid and the reaction was maintained under ice–water conditions for 12 h. The emulsion was broken by isopyknic acetone and the resulting composite was washed by HCl solution, deionized water and ethanol, and then dried at 60 °C under vacuum to obtain the hollow $ZnFe_2O_4$@ PANI composites. The overall materials preparation procedure and the TEM images of the hollow $ZnFe_2O_4$@ PANI composites are schematically illustrated in Fig.9.

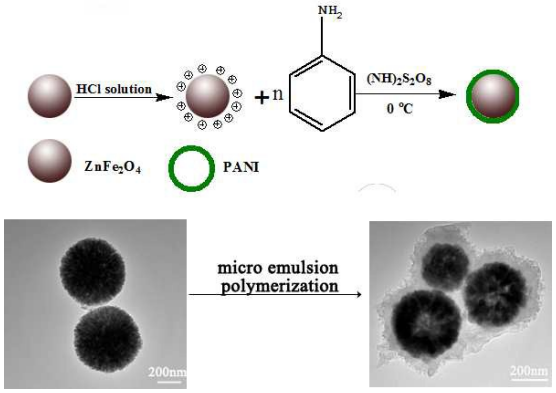

Fig.9 Schematic illustration of the fabrication process for the hollow $ZnFe_2O_4$@PANI composites, and the TEM images of the hollow $ZnFe_2O_4$ nanospheres and hollow $ZnFe_2O_4$@PANI composites.

Preparation of the electrode: Electrochemical performance of the products was evaluated by a CR2016-type coin cell with a multi-channel current static system Land (LAND CT200IA). The anode electrodes were prepared by dispersing the hollow $ZnFe_2O_4$@PANI composites (65wt. %), acetylene black (15wt. %) and PVDF (20wt. %) as a binder in 1-methyl-2-pyrrolidinone (NMP) solution on a copper foil. Li foil was used as the counter-electrode, and polypropylene (PP) film (Celgard 2400) as the separator. The electrolyte solution was 1M $LiPF_6$ dissolved in a mixture of ethylene carbonate (EC), dimethyl carbonate (DMC) and diethyl carbonate (DEC) with a volume ratio of 1:1:1.

Materials characterization: The structures of the prepared samples were characterized by X-ray diffraction analysis (XRD) (Rigaku, model D/max-2500 system at 40 kV and 100 mA of Cu Kα). Thermal analysis of the composite was performed by thermal gravimetric analysis (TGA) (Model Q50, TA, USA) under an air atmosphere, with a heating rate of 20 °C /min, and the temperature range was from 20 to 800 °C. The surface morphology of the composites were performed by a model Tecnai F30 G2 (FEI CO., USA) field emission transmission electron microscope (FETEM) and scanning electron microscope (SEM, SuPRA 55, German ZEISS).

Conclusions:

In summary, the hollow $ZnFe_2O_4$@PANI composites have been successfully synthesized by a micro emulsion polymerization way. The composites show improved cycling stability and rate capability compared to bare $ZnFe_2O_4$. The enhancement in cycling stability could be attributed to the synergetic effect between the highly conductive PANI matrix and hollow structural features. The amorphous PANI and hollow structure in the composites can provide free space to buffer the release of the stress caused by the drastic volume variation during the conversion process. The PANI also offers 3D conductive networks, facilitates the wetting of the active material, and disperses the nanospheres, leading to improved rate capability. As a result, the as-obtained hollow $ZnFe_2O_4$@PANI composites will be a promising anode material for Li-ion batteries.

Acknowledgements

This work was supported by the Research Fund for the Doctoral Program of Higher Education of China under Grant No. 20136102110046, the Innovation Foundation of Shanghai Aero-space Science and Technology Grant No. SAST201373, the Basic Research Foundation of Northwestern Polytechnical University under Grant No. JC201269 and the Graduate Starting Seed Fund of Northwestern Polytechnical University no.Z2015003.

Reference

[1] Tarascon, J. M.; Armand, M. *Nature*, 2001, **414**, 359-367.
[2] Mikhaylik, Y. V.; Akridge, J. R. *J. Electrochem. Soc.* 2004, **151**, A1969–A1976.
[3] Whittingham, M. S. *Chem. Rev,*2004, **104**, 4271-4301.
[4] Arico, A. S.; Bruce, P.; Scrosati, B.; Tarascon, J. M.; Van Schalkwijk,

RSC Advances

ARTICL

W. *Nat. Mater,* 2005, **4**, 366-377.
[5] Sun, J.; Huang, Y. Q.; Wang, W. K.; Yu, Z. B.; Wang, A. B.; Yuan, K. G. *Electrochim. Acta,* 2008, **53**, 7084-7088.
[6] Ji, X. L.; Lee, K. T.; Nazar, L. F. Nat. Mater. 2009, 8 (6), 500–506.V. Etacheri, R. Marom, R. Elazari, G. Salitra and D. Aurbach, *Energy Environ. Sci* ,2011, **4**, 3243.
[7] V. Etacheri, R. Marom, R. Elazari, G. Salitra and D. Aurbach, *Energy Environ. Sci* ,2011, **4**, 3243.
[8] T. H. Kim, J. S. Park, S. K. Chang, S. Choi, J. H. Ryu and H. K. Song, *Adv. Energy Mater* ,2012, **2**, 860.
[9] Y. Chen, H. Xia, L. Lu and J. Xue, *J. Mater. Chem* 2012, 22,5006.
[10] Y. He, L. Huang, J. S. Cai, X. M. Zheng and S. G. Sun, *Electrochim. Acta* ,2010, **55**, 1140
[11] G. Huang, F. Zhang, L. Zhang, X. Du, J. Wang and L. Wang, *J. Mater. Chem. A,* 2014, **2**, 8048.
[12] A. K. Rai, J. Gim, T. V. Thi, D. Ahn, S. J. Cho and J. Kim, J. Phys. Chem. C, 2014, **118**, 11234.
[13] J. Bai, X. Li, G. Liu, Y. Qian and S. Xiong, *Adv. Funct. Mater,* 2014, **24**, 3012.
[14] J. Haetge, C. Suchomski and T. Brezesinski, *Inorg. Chem,* 2010, **49**, 11619.
[15] P. F. Teh, Y. Sharma, S. S. Pramana and M. Srinivasan,*J. Mater. Chem,* 2011, **21**, 14999.
[16] L. Lin and Q. M. Pan, *J. Mater. Chem. A,* 2015, **3**, 1724-1729.
[17] P. F. Teh, Y. Sharma, S. S. Pramana and M. Srinivasan, *J. Mater. Chem*, 2011, **21**, 14999–15008.
[18] F. Mueller, D. Bresser, E. Paillard, M. Winter and S. Passerini, *J. Power Sources,* 2013, **236**, 87-94.
[19] 14 B. J. Li, H. Q. Cao, J. Shao, G. Q. Li, M. Z. Qu and G. Yin, *Inorg. Chem*, 2011, **50**, 1628-1632.
[20] J. F. Li, J. Z. Wang, X. Liang, Z. J. Zhang, H. K. Liu, Y. T. Qian and S. L. Xiong, *ACS Appl. Mater. Interfaces,* 2014, **6**, 24-30.
[21] J. F. Li, J. Z. Wang, D. Wexler, D. Q. Shi, J. W. Liang, H. K. Liu, S. L. Xiong and Y. T. Qian, *J. Mater. Chem. A,* 2013, **1**, 15292-15299.
[22] H. Xia, Y. Qian, Y. Fu and X. Wang, *Solid State Sci* 2013, 17,67.
[23] J. Xie, W. Song, G. Cao, T. Zhu, X. Zhao and S. Zhang, *RSC Adv,* 2014, **4**, 7703.
[24] A. S. Hameed, H. Bahiraei, M. V. Reddy, M. Z. Shoushtari, J. J. Vittal, C. K. Ong and B. V. Chowdari, *ACS Appl. Mater. Interfaces,* 2014, **6**, 10744.
[25] X. Guo, X. Lu, X. Fang, Y. Mao, Z. Wang, L. Chen, X. Xu, H. Yang and Y. Liu, *Electrochem. Commun,* 2010, **12**, 847.
[26] P. Si, S.J. Ding, X.W. Lou, D.H. Kim, *RSC Advances,* 2011, **1** 1271-1278.
[27] Y. Wang, Y. Huang, Q. Wang, Q. He, L. Chen, *Applied Surface Science,* 2012, **259**,486–493.
[28] Y. N. NuLi, Y. Q. Chu and Q. Z. Qin, *J. Electrochem. Soc,* 2004,**151**, A1077–A1083.
[29] D.Y. Chen, G. Ji, Y. Ma, J.Y. Lee, J.M. Lu, *Appl. Mater. Interfaces* ,2011, **3**, 3078–3083.
[30] Q.C. Chen, Q.S. Wu, *J. Hazard. Mater,* 2015, **283**,193–201.
[31] F. Jaouen, J. Herranz, M. Lefevre, J. P. Dodelet, U. I. Kramm,I. Herrmann, P. Bogdanoff, J. Maruyama, T. Nagaoka, A. Garsuch, J. R. Dahn, T. Olson, S. Pylypenko, P. Atanassov and E. A. Ustinov, *ACS Appl. Mater. Interfaces,* 2009, **1**, 1623.
[32] R. L. Arechederra, K. Artyushkova, P. Atanassov and S. D. Minteer, *ACS Appl. Mater. Interfaces,* 2010, **2**, 3295.
[33] E.T. Kang, K.G. Neoh and K.L. Tan, *Prog. Polym. Sci,* 1998, **23**, 277–324.
[34] P. Zhang, Y. Zhan, B. Cai, C. Hao, J. Wang, C. Liu, Z. Meng, Z. Yin, Q. Chen, *Nano Res,* 2010, **3**, 235–243.
[35] Z.J. Du, S.C. Zhang, T. Jiang, X.M. Wu, L. Zhang, H. Fang, *Journal of Power Sources*,2012,**219**,199–203.
[36] Y. Sharma, N. Sharma, G. V. S. Rao and B. V. R. Chowdari, *Electrochim. Acta,* 2008, **53**, 2380.
[37] Y. Chen, M. Zhuo, J. Deng, Z. Xu, Q. Li, T. Wang, J. Mater. Chem A, 2014, 2, 4449-4456.
[38] Y. Ding, Y. F. Yang and H. X. Shao, *Electrochim. Acta,* 2011, **56**, 9433–9438.

Abstract

$ZnFe_2O_4$, a kind of mixed transition metal oxides, are considered as one of the most attractive potential anode materials for LIBs due to their high reversible capacity and satisfactory structural stability. However, the low conductivity and the serious volume exchange during the electrochemical process are still two main issues for $ZnFe_2O_4$. In this study, we firstly designed the conductive PANI layer coated hollow $ZnFe_2O_4$ nanospheres by a micro emulsion polymerization. Two strategies of hollow structure and PANI coating are attempted to relieve expansion and increase conductivity. The results show that as-designed hollow $ZnFe_2O_4$ @PANI composites exhibit a large initial specific capacity of 1489.38mAh g^{-1} at first discharge that is maintained at over 607.3 mAh g^{-1} even after 50 charge-discharge cycles.

Schematic illustration